Molecular Recognition and Supramolecular Self-Assembly of a Genetically Engineered Gold Binding Peptide on Au{111}

Christopher R. So,[†] John L. Kulp III[‡] , Ersin Emre Oren,[†] Hadi Zareie,[†] Candan Tamerler,[†] John Spencer Evans,[‡] and Mehmet Sarikaya[†,*]

[†]Genetically Engineered Materials Science and Engineering Center, Department of Materials Science and Engineering, University of Washington, Seattle, Washington 98105, and [‡]Laboratory for Chemical Physics, New York University, 345 East 24th Street, New York, New York 10010

The biological interactions responsible for structuring and sustaining life occur between molecular entities *via* mechanisms of molecular recognition.[1] Elegant architectures often found in hard biomineralized tissues, for example, are a result of molecular recognition resulting in the formation of hierarchical functional inorganic structures mediated by proteins and other biomolecules.[2,3] Similarly, development of advanced implants and therapeutic devices depends on the biocompatibility of solid surfaces, again at the biomolecule/material interfaces.[4] Consequently, there has been a recent surge in the utilization of the structural and chemical diversity of amino acids to discover sequences with desired material specificity and to utilize these peptides in technology and medicine.[5] At the heart of these diverse fields lies the need for understanding of the mechanism(s) by which specific protein sequences coherently interface with specific solid surfaces.

Combinatorial genetic techniques[6−8] permit isolation of specific recognition elements for surfaces, including those not recognized by naturally occurring amino acid sequences.[9−16] Recently, a number of inorganic binding polypeptide sequences have been selected using combinatorial mutagenesis.[9−16] In our experiments, GBP[1], a gold-binding peptide, was used with an amino acid sequence MHGKTQATSGTIQS, repeated three times to enhance its binding affinity.[9,10] Gold-binding sequences had been isolated as extracellular loops of maltoporin.[9] The binding motif does not contain cysteine residues, known to form Au−thiol linkages with surface atoms, as in self-assembled monolayer (SAM) systems.[17,18]

The solution structure of 3rGBP[1] is intrinsically disordered and consists of a repetitive random coil-extended structure conformation [*i.e.*, (MHGKTQA)$_{random coil}$ −(TSGTIQS)$_{extended}$].[19] This peptide has an interesting dual character: 3rGBP[1] has been shown to both nucleate gold crystals from Au(III) ions in solution as well as preferentially inhibit the growth of the Au{111} crystal face in solution.[10] Investigation of the adsorption of 3rGBP[1] on Au reveals that

ABSTRACT The understanding of biomineralization and realization of biology-inspired materials technologies depends on understanding the nature of the chemical and physical interactions between proteins and biominerals or synthetically made inorganic materials. Recently, combinatorial genetic techniques permit the isolation of peptides recognizing specific inorganic materials that are used as molecular building blocks for novel applications. Little is known about the molecular structure of these peptides and the specific recognition mechanisms onto their counterpart inorganic surfaces. Here, we report high-resolution atomic force microscopy (AFM), molecular simulation (MS), and geometrical docking studies that detail the formation of an ordered supramolecular self-assembly of a genetically engineered gold binding peptide, 3rGBP[1] ([MHGKTQATSGTIQS]$_3$), correlating with the symmetry of the Au{111} surface lattice. Using simulated annealing molecular dynamics (SA/MD) studies based on nuclear magnetic resonance (NMR), we confirmed the intrinsic disorder of 3rGBP[1] and identified putative Au docking sites where surface-exposed side chains align with both the <110> and <211> Miller indices of the Au lattice. Our results provide fundamental insight for an atomistic understanding of peptide/solid interfaces and the intrinsic disorder that is inherent in some of these peptide sequences. Analogous to the well-established atomically controlled thin-film heterostructure formation on semiconductor substrates, the basis of today's microelectronics, the fundamental observations of peptide−solid interactions here may well form the basis of peptide-based hybrid molecular technologies of the future.
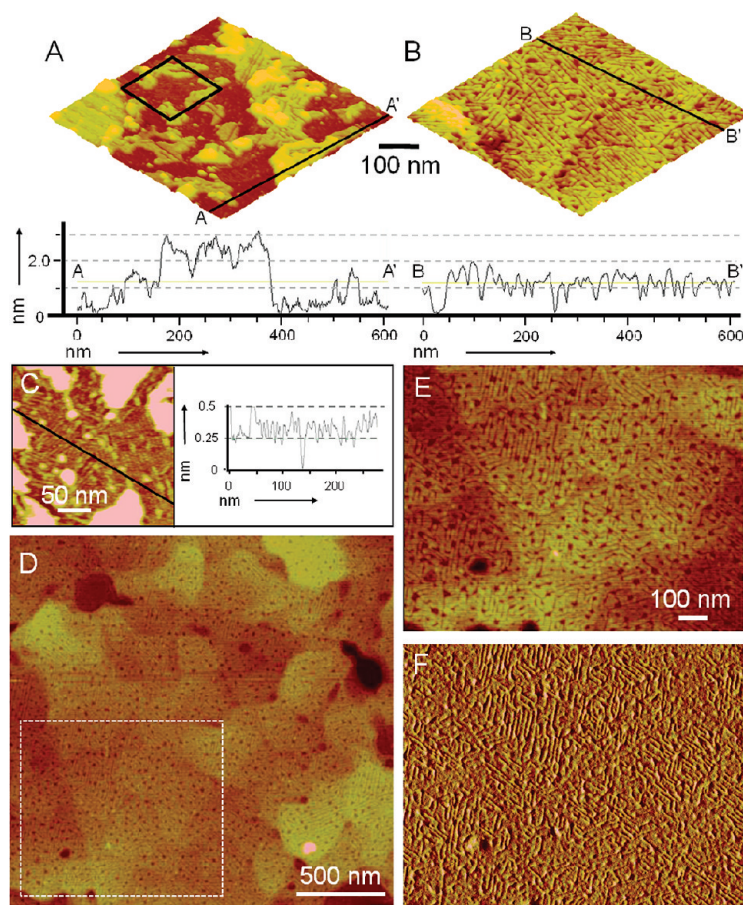
Figure 1. Atomic force microscopy observation of the 3rGBP$_1$ ordered supramolecular assembly on Au{111}. Pseudo-three-dimensional AFM images of the partial (A) and confluent (B) structured layers. The line profiles corresponding to the AFM images show step heights of a harshly rinsed surface (A) compared to one minimally rinsed (B). (C) High-resolution imaging of finely corrugated six-fold symmetrical structures observed on the reconstructed {111} oriented gold surface (from the area outlined by the black square in A), seen to transfer through the overlaying peptide film partially covering the substrate. (D−F) AFM scan over an area of 4 μm^2 showing the long-range ordering of the peptide film on several <111> oriented gold grains, in both height (D,E) and amplitude (F) imaging modes. The self-assembled peptide monolayer has six-fold symmetry in registry with the underlying Au{111} surface lattice.

peptide surface adsorption follows a Langmuir model with specific kinetic parameters (*e.g.*, $K_{eq} \sim 10^7$ M^{-1}) and binding energy ($\Delta G_B \sim -8.0$ kcal/mol)[20,21] similar to those reported for synthetic-based self-assembled monolayers (Figure 1A).[17,18] The recognition mechanism underlying such affinity has not been studied in detail, and it is not clear how the unfolded state of 3rGBP$_1$ directs the recognition and interaction processes on the Au{111} surface or what molecular features would enable self-associative behavior.

Using high-resolution noncontact mode atomic force microscopy (AFM), we first investigated the morphology of 3rGBP$_1$ thin films prepared over large-grained atomically flat surfaces of Au{111}. Figure 1 reports AFM topography images of the resulting peptide films from two separate assembly and rinsing procedures carried out on gold surfaces exposed to a 1 μg/mL peptide solution. Shown in Figure 1A, the use

of aggressive force in the rinsing stream (see Materials and Methods) reveals step heights in the films which correspond to single and dual increments of ~1.5 nm from the gold surface, similar to the previously observed values.[22] This dimension is indicative of peptides assembled with their longest axis parallel to the surface, an orientation allowing the *ca.* 1.5 nm diameter random coil and extended motifs to satisfy side-chain interactions with the underlying gold surface. Upon closer inspection, the peptide film covers a finely corrugated close-packed structure with a six-fold symmetry shown in Figure 1C, implicit gold surface reconstructions with appropriately corresponding heights of ~2−3 Å and ~6 ± 1 nm peak-to-peak separations.[23] As seen in other deposition systems over Au{111},[24] this structure is observed to transfer to the peptide adlayer, yielding nanodomains of roughly double (12 ± 2 nm) the width and maintaining the six-fold orientation of the underlying surface (Figure 1A,B). The use of a noninvasive rinsing (see Materials and Methods) results in a confluent, structured surface film as seen in Figure 1B,D−F with extended six-fold domains. From these observations, the six-fold organization of 3rGBP$_1$ assemblies, or self-assembled peptides (SAPs), correlates strongly with the six-fold symmetry of the gold surface lattice in Figure 1C, suggestive of a possible lattice correlation mechanism. The SAP patterns formed by the ordered domains can be better revealed using both AFM amplitude and height images of the same regions of the sample (Figure 1E,F, respectively). Since the supramolecularly structured peptide covers nearly the whole Au{111} surface periodically, this new self-assembled monolayer may be considered as peptide-tiling consisting of peptide nanodomains.

To investigate the molecular basis for 3rGBP$_1$ self-association and supramolecular assembly, we performed structure refinement simulations of the 42-AA peptide under implicit solvent conditions (see Materials and Methods) and determined a plausible lowest energy conformational ensemble (10 structures) that fit our previously published target NMR data set.[19] The conformer library ($n = 10$) generated by SA/MD is conformationally heterogeneous, as evidenced by the broad distribution of ϕ and ψ backbone torsion angles obtained for the 10 conformers (Figure 2A). This result is expected based on the knowledge of the reported structural lability of this polypeptide[19] and the presence of six Gly residues, which would introduce loop-like conformational flexibility along the length of the peptide molecule.[25−27] The lowest energy-minima structure obtained from SA/MD simulations appears to be intrinsically disordered and possesses an alternating

coil—extended β-strand structure (average chain length = 42 Å), and this result is consistent with the experimental findings reported in our earlier NMR studies (Figure 2B,C).[19] The topological details of this lowest energy structure are intriguing. First, the alternating coil- or looplike structure of 3rGBP$_1$ generates an open, repetitive or patterned three-dimensional surface topology that features short, alternating, accessible cationic (His, Lys) and anionic (Thr, Ser, Gln) motifs (Figure 2D). Such a peptide molecular architecture would offer a significant interactive surface area that could promote complementary interactions among 3rGBP$_1$ molecules. Second, given the absence of internal folding or internal stabilization *via* side chain−side chain intramolecular interactions within 3rGBP$_1$,[19] many of the residues in 3rGBP$_1$ are not committed to internal stabilization interactions. This implies that the majority of the peptide sequence is potentially available for interactions either with the Au{111} surface and/or neighboring 3rGBP$_1$ molecules resulting in intermolecular associations.

It has been hypothesized that some degree of geometric correlation may occur between the peptide and Au{111} surface or the ordered solvation layer(s) directly above the Au surface.[28] Interestingly, when the number of planar solvent-accessible functional groups (free amines and hydroxyls) is plotted against the longitudinal rotation of the molecule as shown in Figure 3A, a prominent interactive domain can be identified spanning a *ca.* 60° peak in the analysis. Topologically, this orientation allows for conformal contact between an open planar loop structure (red segment, inset of Figure 3A) contributed by the second repeat as well as contacts from the first and third repeats with gold, shown in the inset of Figure 3A, as a putative Au{111} binding domain. From Figure 3B, this domain comprises side-chain heteroatoms of the M1, T11, Q13, S14, T22, S23, T25, and K32 residues. The arrangement of these side-chain heteroatoms is intriguing in that three vectors formed by the side-chain heteroatoms of M1-T22-T25-K32, M1-Q13, and S14-T11 align along the <110> direction, while the other two vectors formed by the side-chain heteroatoms of T11-S23 and Q13-T22 align along the <211> direction on the {111} Au surface (also in Figure 3B). This particular orientation of the peptide with the Au{111} surface lattice contains more peptide−lattice correlation axes than others that could be generated through similar analysis performed along other crystallographic directions (as demonstrated in Supporting Information Figure S2). These crystallographic directions possess six-fold symmetry on the Au{111} surface. The crystallographic alignments seen here, therefore, may be the result of 3rGBP$_1$−Au{111} molecular interactions and relative orientations of the peptide with the under-
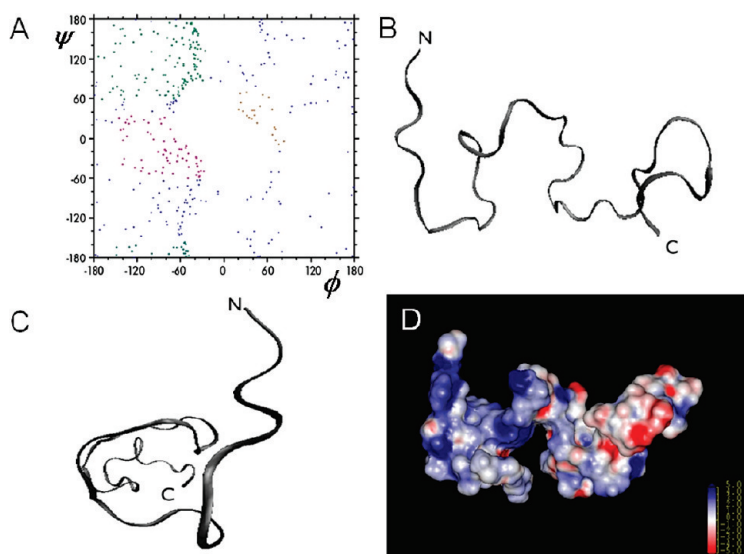

Figure 2. Nuclear magnetic resonance spectroscopy structure and molecular modeling of 3rGBP$_1$. (A) Ramachandran plot of ϕ, ψ torsion angles obtained for the 10 lowest energy 42-AA 3rGBP$_1$ SA/MD conformer ensemble, showing a significantly heterogeneous distribution of structures indicating lability and intrinsic disorder. (B) SA/MD lowest energy minima structure of the 42-AA 3rGBP$_1$ triple repeat, backbone heteroatom representation (ribbon model); (C) as per (B), but observed along the long axis of the polypeptide backbone; (D) as per (B), but heteroatom surface rendering (backbone + side chains), with color scale representing the charge distribution classification (blue = cationic; red = anionic). The letters N and C refer to N- and C-termini, respectively.

lying solid correlating with the observed six-fold symmetrical arrangement of the one-fold symmetrical 3rGBP$_1$ molecule on the Au{111} that are seen in Figure 1.

The ability of 3rGBP$_1$ to form elongated nanodomain assemblies that are crystallographically oriented with the same six-fold symmetry as the Au{111} surface lattice has significant implications for biomimetic nanoscale building strategies on oriented solid material surfaces in general. We believe that the unfolded conformation of 3rGBP$_1$ leads to two characteristics that effectively drive the Au recognition and binding process and, simultaneously, the supramolecular assembly process as well. First, the unfolded state of 3rGBP$_1$ creates an effective surface display of polar (green), nonpolar (white), and cationic (blue) residues (inset of Figure 3B), making it a highly reactive species for both solid Au−peptide interfacial and peptide intermolecular interactions. Moreover, the complementarity between the Au docking surface of 3rGBP$_1$ and the Au{111} interface may direct peptide binding and assembly that parallels the six-fold symmetry of the Au{111} surface (Figures 1 and 3A,B). Second, the unstable, labile conformation of 3rGBP$_1$ also represents a potential driving force for both 3rGBP$_1$−Au{111} and 3rGBP$_1$ self-associative interactions. Given the observed lack of internal stabilization by nonbonding interactions, such as intrachain backbone hydrogen bonding,[19] interactions with the Au{111} or with other 3rGBP$_1$ molecules might provide external stabilization of the peptide conformation and lead to conforma-
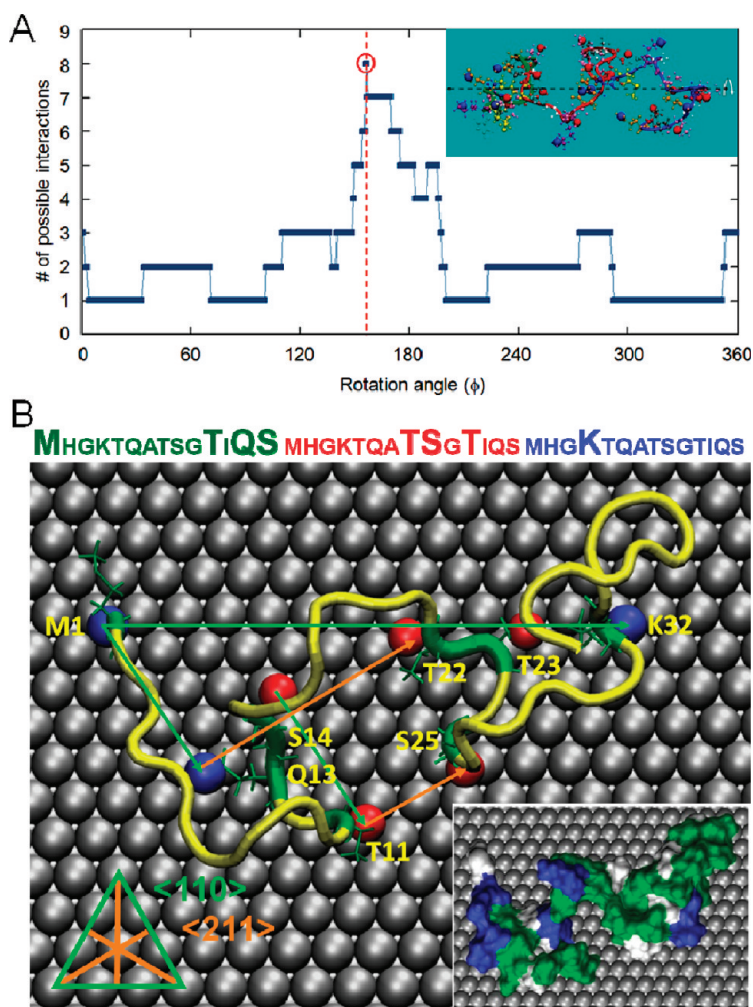
Figure 3. Predicted geometric orientation of 3rGBP₁ on the Au{111} surface. (A) Plot of rotational angle (φ) and number of possible planar interactions between the peptide and the Au{111} surface. The rotation angle, corresponding to the most interactive surface, is indicated by a red circle. The inset shows a representative structure, in which the repeats are labeled by different colors, and the hydrogen bonding donor/acceptor Lys, Thr, Gln, Ser side chain and N-terminus (His) nitrogen (blue) and oxygen (red) atoms are shown individually. (B) Representation of the circled orientation from (A) and its geometric correlation with the {111} surface of gold. The polypeptide backbone is represented in ribbon format (yellow) with docking residues (M1, T11, Q13, S14, T22, S23, T25, and K32, identified along the sequence shown on the top of the figure) highlighted (green) along with their respective heteroatoms involved in surface interactions represented as space-filling atoms in either blue (N) or red (O). The crystallographic directions for specific docking surface atoms are presented in green (<110>) or orange (<211>), depending on their correspondence with the appropriate Miller indices of the Au surface lattice. Inset shows surface representation of potential intermolecular interactions with 3rGBP₁ while bound to Au{111}, highlighting free polar (green), nonpolar (white), and cationic (blue) surfaces.

tional reorganization and internal stabilization throughout the self-assembly process.

The presence of disorder—promoting amino acids such as Gln, Lys, and Ser,[29−31] combined with the presence of disordered or unfolded conformations in solution[19] indicates that 3rGBP₁ is very similar to a class of proteins known as intrinsically disordered proteins (IDP).[29−31] IDPs are now recognized as an independent class of unfolded proteins which possess an array of functions, including assembly and binding to target macromolecules.[29−31] One of the key features of the

IDPs is that these molecules undergo conformational reorganization upon binding to their targets.[31] These features are also common to 3rGBP₁, which may bind to a target with an initial conformation as seen in Figure 3 (e.g., Au surface, other GBP₁ molecules) and further sample conformational space to eventually form an ordered supramolecular array (Figure 1A) over time. The presence of intrinsic disorder, coupled with the reversible nonbonding interactions studied herein, complement recent results[22] showing 3rGBP₁'s ability to be surface-mobile and reconfigure itself at the gold surface to form kinetically favored fibrils during the assembly process. In light of the current study, the directional diffusion of a single molecule, as well as clusters of it throughout the assembly process, may be governed by the number of contacts that a given peptide (having a particular molecular architecture) forms with a certain crystallographic surface of an inorganic solid material. This recognition may inhibit movement along particular directions on the surface while promoting others, allowing the formation of highly ordered long-range and stable peptide films over time. These interactions may, therefore, result in both the observed affinity and selectivity properties of this peptide toward gold surfaces (see Supporting Information Figure S3) over other materials of practical interest.[20,21]

In summary, the peptide 3rGBP₁ represents a new class of biological molecules,[9−16] genetically engineered polypeptides for inorganics (GEPI),[12] that are combinatorially selected to bind to specific inorganics, including metals, oxides, semiconductors, and minerals.[12] The assembly of a GEPI on a surface provides fundamental insight into the molecular recognition of an inorganic by a peptide as illustrated here using a gold-binding peptide on Au{111}. The observed correlation between the peptide and the solid is analogous to the atomically controlled heterostructure formation on semiconductor substrates, the basis of today's microelectronics.[32−34] The observations here may well form the foundation of peptide-based novel hybrid molecular technologies such as protein chips,[35] peptide—nanoparticle conjugates,[12] and designer proteins.[44] Fibrillar structures, similar to elongated nanodomains seen here, are found in a number of biological systems, such as amyloids,[36] collagen,[37] and spider silks,[38] and present an oriented environment for the formation of hierarchical molecular assemblies. Additionally, surface recognition and organization of these molecules provide templates, offering novel practical means over conventional synthetic systems.[39−41] Similar to approaches that utilize organic molecules,

such as thiols on Au,[17,18] a SAP provides an opportunity to build an array of tethered biomacromolecules with recognition or catalytic functions.[40,41] The advantage of utilizing a genetically accessible linking system, furthermore, could also allow *in vivo* manipulation[42–44] for an increase in tagging fidelity and spatial positioning of the solid-affinitive functionality. By using a GEPI, one could utilize multiple sites for fusion with a desired ligand, several ligands of the same type, or several different ligands, increasing binding efficiency and versatility.[42–44] For example, cell surface recognition sequences could be coupled to reactive 3rGBP$_1$ side chains (*e.g.*, Lys) to allow cultured cells to recognize and adhere to Au substrates in cell sorting (*e.g.*, in microfluidics devices).[45] Analogously, important enzymes (*e.g.*, oxidases and reductases)[46] or antibodies could likewise be coupled to assembled 3rGBP$_1$ layers for specific applications. Furthermore, GEPI-based molecular substrates could also be used for selected assembly and controlled organization of nanostructured units,[47] for example, inorganic nanoparticles and nanowires on surfaces, providing a means for molecular fabrication of functional inorganics,[48] a utility in nanotechnology[49,50] and nanomedicine.[41,50]

METHODS AND MATERIALS

Materials. Trifluoroacetic acid (TFA), thioanisole, diethyl ether, anisole, ethanedithiol (EDT), *N,N*-dimethylformamide (DMF), piperidine, *N,N*-diisopropylethylamine (DIEA), and acetonitrile (ACN) were purchased from Sigma-Aldrich (St. Louis, MO). *O*-(1*H*-Benzotriazole-1-yl)-*N,N,N′,N′*-tetramethyluronium hexafluorophosphate (HBTU) was purchased from CS Bio (Menlo Park, CA). Preloaded Wang resin and pseudoproline dipeptides were acquired from Novabiochem (San Diego, CA), while appropriately side-chain-protected Fmoc amino acids were from Chempep (Miami, FL). All peptides were purified using Gemini (Phenomenex, Inc., Torrance, CA) C18 peptide/protein reverse-phase columns for analytical (250 × 4.6 mm, 5 μm particle, 110 Å pore) and semipreparative purification (250 × 21.2 mm, 10 μm particle, 110 Å pore); HPLC solvents used were solvent A (0.1% TFA in water) and solvent B (90% acetonitrile, 10% water, and 0.1% TFA). Peptides were stored and incubated in a 3:1 K$_2$HPO$_4$/KH$_2$PO$_4$ 10 mM phosphate buffer with 100 mM KCl at a pH of 7.00. Concentrated HCl and NaOH solutions were used to establish the desired pH of the sample (Nanopure Milli-Q water (deionized and distilled) was used for the preparation of all solutions unless stated otherwise). Au{111} gold surfaces were purchased from Agilent (Santa Clara, CA).

Peptide Synthesis. Peptides were prepared on an automated solid-phase peptide synthesizer (CS336X, CSBio Inc., Menlo Park, CA) employing standard batchwise Fmoc chemistry procedures. To prevent interchain interactions and a lowering of yield, Fmoc-Ala-Thr($\psi^{Me,Me}$pro)-OH and Fmoc-Gln(Trt)-Ser($\psi^{Me,Me}$pro)-OH pseudoproline dipeptides (Novabiochem, San Diego, CA) were inserted at five permissive locations throughout the sequence. Briefly, synthesis was carried out on a preloaded Fmoc-Ser(tBu)-Wang (Novabiochem, San Diego, CA) low-loading support resin using HBTU activation chemistry, while 20% piperidine in DMF was employed to afford the Fmoc deprotection and monitored by UV absorbance at 301 nm. Following solid-phase synthesis, the peptide was cleaved off the support and side chain deprotected by stirring the resin-bound peptide in a cocktail containing 90:5:3:2 TFA/thioanisole/EDT/anisole under N$_2$ atmosphere for ~6 h. The resin was removed by filtration, and the peptide was precipitated with cold ether to yield crude peptide product that was lyophilized (Virtis Benchtop K, SP Industries, Inc., Warminster, PA). Reconstitution of the peptide powder required immersion in 50 μL of TFA followed by ~40/60 vol %. ACN to DI H$_2$O. Purification by reverse-phase HPLC for 3rGBP$_1$ employed first an isocratic (0% B for 2 min) then a linear gradient of 1%/min for analytical and 0.5%/min for semiprep scales at 1 and 10 mL/min flow rates, respectively. Retention times were *ca.* 38 min for semiprep and *ca.* 27 min for analytical. Analytical peaks were isolated by autothreshold collection (Waters Deltaprep 600, analytical mode) and were identified by MALDI-TOF mass spectrometry with reflectron (RETOF-MS) on an Autoflex II (Bruker Daltonics, Billerica, MA) mass spectrometer in positive-ion mode, and the observed 3403.4 M/Z fraction was subsequently collected manually from the scaled semipreparative separation (Waters Deltaprep 600, semiprep mode). Representative chromatogram

and its mass spectrum of the resultant pure peptide can be found in the Supporting Information (Figure S4).

AFM Sample Preparation. The 150 nm thick {111} oriented gold substrates were hydrogen flame annealed prior to use *via* the protocol established by the manufacturer to clean off any organic contaminants and retain pristine gold surfaces for immediate use. For assembly, the gold substrates were cut to 3 mm^2 squares and fully submerged in 3rGBP$_1$ solution with a peptide concentration of 1 μg/mL for 20 min. Immediately after incubation, substrates were removed from the solution and sprayed with a stream of DI water from a soft water bottle at varying forces. For light rinsing, water was dripped at a rate of ~1 drop/s, while heavy rinsing involved grasping the water bottle with considerable force. Surfaces were rinsed for 1 min before thoroughly blow drying in argon and scanned.

AFM Measurements. A Digital Instruments (Santa Barbara, CA) Multimode Nanoscope IIIa scanning probe microscope equipped with high frequency NanoSensors PPP-NCHR (NanoandMore USA, Lady's Island, SC) noncontact probes with a 42 N/m spring constant were used to scan the Au{111} surface. All imaging was carried out under tapping mode, with 512 × 512 data acquisitions at a scan speed of 0.8 Hz at room temperature under positive N$_2$ pressure under acoustic isolation. Supplier-provided software (Nanoscope, V5.3r1, Veeco) was utilized for extracting quantitative data such as surface cross sections from AFM images. For high-resolution imaging, only tips with observed radii nominally <5 nm were used on individual gold grains ranging from 200 to 400 nm and magnified so that there was one single atomically flat surface to perform first order *XY* plane fitting. After images were collected, average feature widths were quantified by measuring the peak-to-peak distances over the span of multiple fibers. One hundred samples were taken over multiple images for each dimension from both substrates. Images were analyzed either as height or amplitude display modes.

Simulated Annealing Molecular Dynamics (SA/MD). Initial polypeptide coordinates were generated in the biopolymer module (Biosym InsightII package, Accelrys, San Diego, USA) using the CVFF force field and extended conformation ($\phi = 0°$, $\psi = 0°$). Side chain partial atomic charges (protonated Lys, His side chain groups, ε-NH$_3^+$ and COO$^-$ termini) were explicitly represented to emulate a neutral pH scenario (net charge = +6). NOE values obtained for the single repeat[19] were used as restraints in setting corresponding H—H distances and dihedral angles at specific locations within the first, second, and third repeat regions of this starting structure (Table 1 of ref 22), using a build-up strategy similar to that employed in our previous work.[25] For example, backbone restraints experimentally obtained for Met1 in the single repeat were applied to Met1, Met 15, and Met 29 in the triple repeat; His2 was applied to His16, His30, and so on. NMR distance restraints were applied as either strong (1.8—2.5 Å), medium (2.5—3.5 Å), or weak (3.5—5.0 Å) soft-square potentials with force constant of 50 kcal/mol · Å^2. Inter- and intraresidue interproton distances were calculated using a reference distance of 2.4 Å for Ala α-CH-β-CH protons.[25] Pseudoatoms defining the centroids of the methyl and methylene groups were defined in the NOE restraint file. Due to the conformational lability of 3rG-

BP$_1$, only a total of 96 NOE restraints were available (18 inter-residue and 78 intraresidue restraints). All other H−H distances were left unrestrained in the starting structure. Simulated annealing molecular dynamics runs (10 total) were conducted using the XPLOR software package; specifically, all simulations employed a distance-dependent dielectric ($\varepsilon = 78.5$, representing implicit solvation, using a nonbonding cutoff of 4.5 Å to determine electrostatic interactions using a switching function), and the Verlet algorithm integrator was used (1 fs per step) along with a temperature coupling option. Essentially, this approach is a Langevin-type dynamics method with zero random forces and a scaled friction coefficient. Following initial minimization to convergence (Fletcher−Powell algorithm), 30 ps of equilibrium dynamics were performed at 300 K, and then the system was incrementally ramped to 2000 K to sample conformational space. The system was cooled from 2000 at 100 K per step to 300 K, and the resulting conformers were then minimized to convergence. Peptide coordinate files were visualized using the Visual Molecular Dynamics software package (Humphrey, W. *J. Mol. Graph.* **1996**, *14*, 33−38). Connolly surface calculations were done by nonlinear solution to the Poisson−Boltzmann (PB) equation *via* DELPHI (Accelrys, San Diego, CA). The dielectric constants were set to 4 for solute molecules and 80 for the solvent. The solvent radius and ionic radius were defined as 1.4 and 2.0 Å, respectively, and a grid size of 257 was utilized. Approximate convergence of the nonlinear Poisson−Boltzmann equation was obtained after 800 iterations. The solvent-accessible area and solvation energies were calculated using a 1.4 Å probe. The electrostatic surface maps in Figure 2D were analyzed with InsightII (MSI/Biosym).

Geometric Docking of 3rGBP$_1$ on Au{111}. To determine if the SA/MD lowest energy structure possesses some degree of geometric complementarity with the Au{111} surface, we performed polypeptide surface alignment studies. We first aligned the longest dimension of the lowest energy conformer of 3rGBP$_1$ along the *y*-axis parallel to the substrate, and then we rotated the conformer horizontally along the *y*-axis in 1° increments (360° total). At each increment, we examined the conformer for planar arrangements of hydrogen bonding donor/acceptor Lys, Thr, Gln, and Ser side chain and NH$_3^+$ main chain nitrogen and oxygen atoms, which could hypothetically form nonbonding interactions with the Au{111} interface or with surface-adsorbed water molecules directly above this interface (Supporting Information Figure S1). The configuration that had the maximum number of possible interactions (8: M1, T11, Q13, S14, T22, S23, T25, and K32 residues) was identified and termed as the docking surface.

Using a Au{111} surface that was constructed from lattice cell parameters for crystalline gold (4.0782 Å), this docking surface was initially positioned above the Au{111} surface and then repositioned to provide the best geometric fit between the docking surface and the Au atoms at the {111} surface. To find the best fit, we first calculate projected distances between the interaction points onto the Au{111} surface (Supporting Information Table S1) and then normalize them by each nearest neighbor distance given in Supporting Information Table S2. If the distance between any given two interaction atoms is an integer multiple (within a 99% confidence limit) of the nearest neighbor distance on the Au{111} surface, then these two atoms are assumed to align along the corresponding crystallographic direction on the metal surface. On the basis of these criteria, a list of lattice (spatial) match between the 3rGBP$_1$ and Au{111} surface has been found and listed in Supporting Information Table S3. The docking corresponding to the highest number of alignments has three vectors formed by side-chain heteroatoms of M1-T22, M1-K32, and T25-K32, align along the <110> direction with a distance integer multiple of the unit length of the corresponding crystallographic direction. As shown in Figure 3B, when the above corresponding side-chain heteroatoms of 3rGBP$_1$ aligned along the <110> direction, the following four more alignments also observed altogether lead to formation of six-fold symmetry observed in experiments: M1-Q13 and S14-T11 align along the <110> direction, while the other two side-chain heteroatoms of T11-S23 and Q13-T22 align along the <211> direction on the {111} oriented gold substrate.

REFERENCES AND NOTES

1. Pauling, L. Molecular-Basis of Biological Specificity. *Nature* **1974**, *248*, 769–771.
2. Lowenstam, H. A.; Weiner, S. Biomineralization Processes. In *On Biomineralization*; Oxford University Press: New York, 1989; pp 25−41.
3. Mann, S. *Biomimetic Materials Chemistry*; VCH: New York, 1996.
4. Horbett T.A.; Brash, J. L. *Proteins at Interfaces II: Fundamentals and Applications*; American Chemical Society: Washington, DC, 1995.
5. Sarikaya, M. Biomimetics: Materials Fabrication through Biology. *Proc. Natl. Acad. Sci. U.S.A.* **1999**, *96*, 14183–14185.
6. Smith, G. P. Filamentous Fusion Phage: Novel Expression Vectors that Display Cloned Antigens on the Virion Surface. *Science* **1985**, *228*, 1315–1317.
7. Hoess, R. H. Protein Design and Phage Display. *Chem. Rev.* **2001**, *101*, 3205–3218.
8. Wittrup, K. D. Protein Engineering by Cell-Surface Display. *Curr. Opin. Biotechnol.* **2001**, *12*, 395–399.
9. Brown, S. Metal-Recognition by Repeating Polypeptides. *Nat. Biotechnol.* **1997**, *15*, 269–272.
10. Brown, S.; Sarikaya, M.; Johnson, E. A Genetic Analysis of Crystal Growth. *J. Mol. Biol.* **2000**, *299*, 725–735.
11. Whaley, S. R.; English, D. S.; Hu, E. L.; Barbara, P. F.; Belcher, A. M. Selection of Peptides with Semiconductor Binding Specificity for Directed Nanocrystal Assembly. *Nature* **2000**, *405*, 665–668.
12. Sarikaya, M.; Tamerler, C.; Jen, A. K. Y.; Schulten, K.; Baneyx, F. Molecular Biomimetics: Nanotechnology through Biology. *Nat. Mater.* **2003**, *2*, 577–585.
13. Naik, R. R.; Brott, L. L.; Clarson, S. J.; Stone, M. O. Silica-Precipitating Peptides Isolated from a Combinatorial Phage Display Peptide Library. *J. Nanosci. Nanotechnol.* **2002**, *2*, 95–100.
14. Kjaergaard, K.; Schembri, M. A.; Klemm, P. Novel Zn^{2+}-Chelating Peptides Selected from a Fimbria-Displayed Random Peptide Library. *Appl. Environ. Microbiol.* **2001**, *67*, 5467–5473.
15. Gaskin, D. J. H.; Starck, K.; Vulfson, E. N. Identification of Inorganic Crystal-Specific Sequences Using Phage Display Combinatorial Library of Short Peptides: A Feasibility Study. *Biotechnol. Lett.* **2000**, *22*, 1211–1216.
16. Lee, S. W.; Mao, C. B.; Flynn, C. E.; Belcher, A. M. Ordering of Quantum Dots Using Genetically Engineered Viruses. *Science* **2002**, *296*, 892–895.
17. Whitesides, G. M.; Mathias, J. P.; Seto, C. T. Molecular Self-Assembly and Nanochemistry: A Chemical Strategy for the Synthesis of Nanostructures. *Science* **1991**, *254*, 1312–1319.
18. Schreiber, F. Structure and Growth of Self-Assembling Monolayers. *Prog. Surf. Sci.* **2000**, *65*, 151–256.
19. Kulp, J. L.; Sarikaya, M.; Evans, J. S. Molecular Characterization of a Prokaryotic Polypeptide Sequence that Catalyzes Au Crystal Formation. *J. Mater. Chem.* **2004**, *14*, 2325–2332.
20. Tamerler, C.; Oren, E. E.; Duman, M.; Venkatasubramanian, E.; Sarikaya, M. Adsorption Kinetics of an Engineered Gold Binding Peptide by Surface Plasmon Resonance Spectroscopy and a Quartz Crystal Microbalance. *Langmuir* **2006**, *22*, 7712–7718.

21. Seker, U. O. S.; Wilson, B.; Sahin, D.; Tamerler, C.; Sarikaya, M. Quantitative Affinity of Genetically Engineered Repeating Polypeptides to Inorganic Surfaces. *Biomacromolecules* **2009**, *10*, 7.

22. So, C. R.; Tamerler, C.; Sarikaya, M. Adsorption, Diffusion, and Self-Assembly of an Engineered Gold-Binding Peptide on Au(111) Investigated by Atomic Force Microscopy. *Angew. Chem., Int. Ed.* DOI: 10.1002/anie.200805259.

23. Fujita, D.; Amemiya, K.; Yakabe, T.; Nejoh, H.; Sato, T.; Iwatsuki, M. Anisotropic Standing-Wave Formation on an Au(111)-(23x Root 3) Reconstructed Surface. *Phys. Rev. Lett.* **1997**, *78*, 3904–3907.

24. Chambliss, D. D.; Wilson, R. J.; Chiang, S. Nucleation of Ordered Ni Island Arrays on Au(111) by Surface-Lattice Dislocations. *Phys. Rev. Lett.* **1991**, *66*, 1721–1724.

25. Zhang, B.; Wustman, B. A.; Morse, D.; Evans, J. S. Model Peptide Studies of Sequence Regions in the Elastomeric Biomineralization Protein, Lustrin A. I. The C-Domain Consensus-Pg-, -Nvnct-Motif. *Biopolymers* **2002**, *63*, 358–369.

26. Datta, S.; Shamala, N.; Banerjee, A.; Balaram, P. Conformational Variability of Gly-Gly Segments in Peptides: A Comparison of the Crystal Structures of an Acyclic Pentapeptide and an Octapeptide. *Biopolymers* **1997**, *41*, 331–336.

27. Wustman, B. A.; Santos, R.; Zhang, B.; Evans, J. S. Identification of a "Glycine-Loop"-like Coiled Structure in the 34 AA Pro, Gly, Met Repeat Domain of the Biomineral-Associated Protein, Pm27. *Biopolymers* **2002**, *65*, 362–372.

28. Braun, R.; Sarikaya, M.; Schulten, K. Genetically Engineered Gold-Binding Polypeptides: Structure Prediction and Molecular Dynamics. *J. Biomater. Sci., Polym. Ed.* **2002**, *13*, 747–757.

29. Uversky, V. N. Natively Unfolded Proteins: A Point Where Biology Waits for Physics. *Protein Sci.* **2002**, *11*, 739–756.

30. Dyson, H. J.; Wright, P. E. Nuclear Magnetic Resonance Methods for Elucidation of Structure and Dynamics in Disordered States. *Nucl. Magn. Reson.* **2001**, *339*, 258–270.

31. Tompa, P. Intrinsically Unstructured Proteins. *Trends Biochem. Sci.* **2002**, *27*, 527–533.

32. Brune, H. Microscopic View of Epitaxial Metal Growth: Nucleation and Aggregation. *Surf. Sci. Rep.* **1998**, *31*, 121–229.

33. Mo, Y. W.; Kleiner, J.; Webb, M. B.; Lagally, M. G. Activation-Energy for Surface-Diffusion of Si on Si(001): A Scanning-Tunneling-Microscopy Study. *Phys. Rev. Lett.* **1991**, *66*, 1998–2001.

34. Venables, J. A. Rate Equation Approaches to Thin-Film Nucleation Kinetics. *Philos. Mag.* **1973**, *27*, 697–738.

35. Templin, M. F.; Stoll, D.; Schrenk, M.; Traub, P. C.; Vohringer, C. F.; Joos, T. O. Protein Microarray Technology. *Trends Biotechnol.* **2002**, *20*, 160–167.

36. DePace, A. H.; Santoso, A.; Hillner, P.; Weissman, J. S. A Critical Role for Amino-Terminal Glutamine/Asparagine Repeats in the Formation and Propagation of a Yeast Prion. *Cell* **1998**, *93*, 1241–1252.

37. Timpl, R.; Brown, J. C. Supramolecular Assembly of Basement Membranes. *BioEssays* **1996**, *18*, 123–132.

38. Kaplan, D.; Adams, W. W.; Farmer, B.; Viney, C. Silk - Biology, Structure, Properties, and Genetics. *Silk Polym.* **1994**, *544*, 2–16.

39. Daniel, M. C.; Astruc, D. Gold Nanoparticles: Assembly, Supramolecular Chemistry, Quantum-Size-Related Properties, and Applications toward Biology, Catalysis, and Nanotechnology. *Chem. Rev.* **2004**, *104*, 293–346.

40. Hamley, I. W. Nanotechnology with Soft Materials. *Angew. Chem., Int. Ed.* **2003**, *42*, 1692–1712.

41. Langer, R.; Peppas, N. A. Advances in Biomaterials, Drug Delivery, and Bionanotechnology. *AIChE J.* **2003**, *49*, 2990–3006.

42. McMillan, R. A.; Paavola, C. D.; Howard, J.; Chan, S. L.; Zaluzec, N. J.; Trent, J. D. Ordered Nanoparticle Arrays Formed on Engineered Chaperonin Protein Templates. *Nat. Mater.* **2002**, *1*, 247–252.

43. Klem, M. T.; Willits, D.; Solis, D. J.; Belcher, A. M.; Young, M.; Douglas, T. Bio-Inspired Synthesis of Protein-Encapsulated Copt Nanoparticles. *Adv. Funct. Mater.* **2005**, *15*, 1489–1494.

44. Dai, H. X.; Choe, W. S.; Thai, C. K.; Sarikaya, M.; Traxler, B. A.; Baneyx, F.; Schwartz, D. T. Nonequilibrium Synthesis and Assembly of Hybrid Inorganic-Protein Nanostructures Using an Engineered DNA Binding Protein. *J. Am. Chem. Soc.* **2005**, *127*, 15637–15643.

45. Quake, S. R.; Scherer, A. From Micro- to Nanofabrication with Soft Materials. *Science* **2000**, *290*, 1536–1540.

46. Baldwin, A. J.; Bader, R.; Christodoulou, J.; MacPhee, C. E.; Dobson, C. M.; Barker, P. D. Cytochrome Display on Amyloid Fibrils. *J. Am. Chem. Soc.* **2006**, *128*, 2162–2163.

47. Zin, M. T.; Munro, A. M.; Gungormus, M.; Wong, N. Y.; Ma, H.; Tamerler, C.; Ginger, D. S.; Sarikaya, M.; Jen, A. K. Y. Peptide-Mediated Surface-Immobilized Quantum Dot Hybrid Nanoassemblies with Controlled Photoluminescence. *J. Mater. Chem.* **2007**, *17*, 866–872.

48. Slocik, J. M.; Tam, F.; Halas, N. J.; Naik, R. R. Peptide-Assembled Optically Responsive Nanoparticle Complexes. *Nano Lett.* **2007**, *7*, 1054–1058.

49. Cui, Y.; Lieber, C. M. Functional Nanoscale Electronic Devices Assembled Using Silicon Nanowire Building Blocks. *Science* **2001**, *291*, 851–853.

50. Tamerler, C.; Sarikaya, M. Molecular Biomimetics: Nanotechnology and Molecular Medicine Utilizing Genetically Engineered Peptides. *Philos. Trans. R. Soc. London, Ser. A*, published online.